Chapter 10
Scaling Flows and Dissipation in the Dilute Fermi Gas at Unitarity

T. Schäfer and C. Chafin

Abstract We describe recent attempts to extract the shear viscosity of the dilute Fermi gas at unitarity from experiments involving scaling flows. A scaling flow is a solution of the hydrodynamic equations that preserves the shape of the density distribution. The scaling flows that have been explored in the laboratory kfIccare the transverse expansion from a deformed trap ("elliptic flow"), the expansion from a rotating trap, and collective oscillations. We discuss advantages and disadvantages of the different experiments, and point to improvements of the theoretical analysis that are needed in order to achieve definitive results. A conservative bound based on the current data is that the minimum of the shear viscosity to entropy density ration is $\eta/s \leq 0.5\hbar/k_B$.

10.1 Introduction

A cold, dilute Fermi gas of non-relativistic spin 1/2 particles interacting via a short range interaction tuned to infinite scattering length, commonly referred to as the unitary Fermi gas, provides a new paradigm for many strongly correlated quantum systems [1, 2]. In this contribution we focus on non-equilibrium aspects of the unitary Fermi gas, in particular its shear viscosity [3]. The shear viscosity of a liquid composed of weakly coupled quasi-particles can be estimated as

$$\eta = \frac{1}{3} n p l_{mfp}, \tag{10.1}$$

T. Schäfer (✉) · C. Chafin
Department of Physics, North Carolina State University,
Raleigh, NC 27695, USA
e-mail: tmschaef@unity.ncsu.edu

C. Chafin
e-mail: cechafin@ncsu.edu

W. Zwerger (ed.), *The BCS–BEC Crossover and the Unitary Fermi Gas*,
Lecture Notes in Physics 836, DOI: 10.1007/978-3-642-21978-8_10,

where n is the density, p is the average momentum of the particles, and l_{mfp} is the mean free path. The mean free path can be written as $l_{mfp} = 1/(n\sigma)$ where σ is the transport cross section. Eq. 10.1 implies that the shear viscosity decreases as the strength of the interaction increases. In the unitary gas the cross section saturates the s-wave unitarity bound $\sigma = 4\pi/k^2$, where k is the scattering momentum, and we expect the shear viscosity to be unusually small.

Danielewicz and Gyulassy pointed out that the Heisenberg uncertainty relation imposes a bound on the product of the average momentum and the mean free path, $pl_{mfp} \geq \hbar$, and concluded that $\eta/n \geq \hbar$ [4]. This is not a precise statement: The kinetic estimate in Eq. 10.1 is not valid if the mean free path is on the order of the mean momentum. A more precise bound has recently emerged from holographic dualities in string theory. In this context the natural quantity to consider is not the ratio η/n, but η/s, where s is the entropy density. Policastro, Son and Starinets showed that in $\mathcal{N} = 4$ supersymmetric QCD the strong coupling limit of η/s is equal to $\hbar/(4\pi k_B)$ [5]. It was later shown that the strong coupling limit is universal in a large class of field theories, and it was conjectured that $\eta/s \geq \hbar/(4\pi k_B)$ is a general lower bound, valid for all fluids [6].

Are there any fluids in nature that attain or possibly violate the proposed bound? A fluid that saturates the bound has to be a quantum fluid (because η is on the order of $\hbar s$), and it has to be strongly interacting (because in a weakly interacting system the mean free path is large). It is also known that many of the model field theories that attain the bound in the strong coupling limit are scale invariant. All of these properties point to the unitary Fermi gas as a plausible candidate for a "perfect fluid".

Almost ideal hydrodynamic flow in the unitary Fermi gas was first observed in [7]. Since then, a number of experiments have been performed that provide constraints on the shear viscosity of the unitary gas [8–15]. In this work we will provide an overview of the hydrodynamic analysis of these experiments, and compare some of the estimates that have been obtained. We emphasize the uncertainties of these results, and point to improvements that need to be implemented.

10.2 Scaling Flows

We begin by studying the ideal (Eulerian) fluid dynamics of a non-relativistic gas in the normal phase. We will introduce dissipative effects in Sects. 10.3.1–10.3.3. In this contribution we will not discuss superfluid hydrodynamics. We will briefly comment on dissipative effects in the superfluid phase in Sect. 10.3.1. The equations of continuity and of momentum conservation are given by

$$\frac{\partial n}{\partial t} + \vec{\nabla} \cdot (n\vec{v}) = 0, \tag{10.2}$$

$$mn\frac{\partial \vec{v}}{\partial t} + mn\left(\vec{v} \cdot \vec{\nabla}\right)\vec{v} = -\vec{\nabla}P - n\vec{\nabla}V, \tag{10.3}$$

where n is the number density, m is the mass of the atoms, $\vec{v}$ is the fluid velocity, P is the pressure and V is the external potential. In the unitarity limit the equation of state at zero temperature is of the form

$$P(n,T) = \frac{n^{5/3}}{m} f\left(\frac{mT}{n^{2/3}}\right), \tag{10.4}$$

where *f(y)* is a universal function. We note that $y = const \cdot (T/T_F^{hom})$, where $T_F^{hom} = (3\pi^2 n)^{2/3}/(2m)$ is the Fermi temperature of a homogeneous Fermi gas. In the high temperature limit, $y \gg 1$, we have $f(y) \simeq y$ and in the low temperature limit $f(y) \simeq (3\pi^2)^{2/3}\xi/5$, where the parameter $\xi = 0.40(2)$ has been determined in quantum Monte Carlo calculations [16]. Monte Carlo methods have also been used to determine *f(y)* for all values of y [17, 18]. The critical temperature for superfluidity is $T_c/T_F^{hom} \simeq 0.15$, corresponding to $y_c \simeq 0.72$. An alternative representation of the pressure is

$$P(\mu,T) = \mu^{5/2} m^{3/2} g\left(\frac{T}{\mu}\right), \tag{10.5}$$

where *g(z)* is a universal function, related to *f(y)* by thermodynamic identities. In the high temperature limit $g(z) \simeq 2z^{5/2}e^{1/z}/(2\pi)^{3/2}$ and in the low temperature limit $g(z) \simeq 2^{5/2}/(15\pi^2\xi^{3/2})$. The density is

$$n(\mu,T) = \mu^{3/2} m^{3/2} h\left(\frac{T}{\mu}\right), \quad h(z) = \frac{5}{2}g(z) - zg'(z). \tag{10.6}$$

The high and low temperature limits of the function *h(z)* are $h(z) \simeq 2z^{3/2}e^{1/z}/(2\pi)^{3/2}$ $(z \gg 1)$ and $h(z) \simeq 2^{3/2}/(3\pi^2\xi^{3/2})(z \ll 1)$. The equilibrium distribution n_0 of a trapped atomic gas follows from the hydrostatic equation $\vec{\nabla}P_0 = -n_0\vec{\nabla}V$. The trapping potential is approximately harmonic

$$V(x) = \frac{m}{2}\sum_i \omega_i^2 x_i^2. \tag{10.7}$$

Using the Gibbs-Duhem relation $dP = nd\mu + sdT$ together with the fact that the equilibrium configuration is isothermal we can write the equation of hydrostatic equilibrium as $\vec{\nabla}\mu = -\vec{\nabla}V$. This implies that the equilibrium density is $n_0(x) = n(\mu(x), T)$ with

$$\mu(x) = \mu_0 - V(x) = \mu_0\left(1 - \sum_i \frac{x_i^2}{R_i^2}\right), \quad R_i^2 = \frac{2\mu_0}{m\omega_i^2}. \tag{10.8}$$

A scaling flow is a solution of the hydrodynamic equations in which the shape of the density distribution is preserved. Consider the ansatz $n(x,t) = n(\mu(x,t), T(t))$ where

$$\mu(x,t) = \mu_0(t)\left(1 - \frac{x^2}{R_x(t)^2} - \frac{y^2}{R_y(t)^2} - \frac{z^2}{R_z(t)^2} - \frac{xy}{R_{xy}(t)}\right), \tag{10.9}$$

and $T(t)/T(0) = \mu_0(t)/\mu_0(0)$. Without loss of generality we have restricted the ansatz to rotations in the xy-plane. We note that the fluid remains isothermal during the expansion. Scale invariance implies that properties of the fluid only depend on the dimensionless ratio T/μ. For any given fluid element this ratio does not change during the expansion. In particular, if the fluid element was in the superfluid or normal phase initially, it will stay in that phase throughout the expansion.

The velocity field created by the scaling expansion in Eq. 10.9 is linear in the coordinates. We can write

$$\vec{v}(x,t) = \frac{1}{2}\vec{\nabla}\left(\alpha_x(t)x^2 + \alpha_y(t)y^2 + \alpha_z(t)z^2 + 2\alpha(t)xy\right) + \Omega(t)\hat{z}\times\vec{x}. \tag{10.10}$$

The parameters α_i, α and Ω are related to the parameters R_i, R_{xy} and μ_0 by the continuity equation. Remarkably, the continuity equation is independent of the universal function *h(z)* in Eq. 10.6. Introducing the dimensionless scale parameters

$$\bar{\mu}(t) = \frac{\mu_0(t)}{\mu_0(0)}, \quad b_i(t) = \frac{R_i(t)}{R_i(0)}, \quad a(t) = \frac{R_x(0)^2}{R_{xy}(t)}, \tag{10.11}$$

the continuity equation can be written as

$$\dot{\bar{\mu}} + \frac{2}{3}\bar{\mu}\left(\alpha_x + \alpha_y + \alpha_z\right) = 0, \tag{10.12}$$

$$\dot{a} + \frac{2(\alpha-\Omega)}{b_x^2} + \frac{2(\alpha+\Omega)}{\lambda^2 b_y^2} + a(\alpha_x+\alpha_y) = 0, \tag{10.13}$$

$$\dot{b}_x - b_x\alpha_x - \frac{b_x^3 a}{2}(\alpha+\Omega) = 0, \tag{10.14}$$

$$\dot{b}_y - b_y\alpha_y - \frac{b_y^3\lambda^2 a}{2}(\alpha-\Omega) = 0, \tag{10.15}$$

$$\dot{b}_z - b_z\alpha_z = 0, \tag{10.16}$$

where $\lambda = R_y(0)/R_x(0) = \omega_x/\omega_y$. These equations can be solved directly in the case that there is no rotation, $a(t) = 0$. Then $\alpha = \Omega = 0$ and

$$(\alpha_x, \alpha_y, \alpha_z) = \left(\frac{\dot{b}_x}{b_x}, \frac{\dot{b}_y}{b_y}, \frac{\dot{b}_z}{b_z}\right), \quad \bar{\mu} = \frac{1}{(b_x b_y b_z)^{2/3}}. \tag{10.17}$$

The velocity field is a simple "Hubble flow", $\vec{v} = (\alpha_x x, \alpha_y y, \alpha_z z)$. Finally, we note that the entropy density is given by $s = (m\mu)^{3/2} g'(T/\mu)$. Since the entropy density

has the same functional form as the particle density we conclude that, in the case of scaling flows, the continuity equation implies entropy conservation,

$$\frac{\partial s}{\partial t} + \vec{\nabla} \cdot (\vec{v} s) = 0. \tag{10.18}$$

10.3 Elliptic Flow

The simplest scaling flow is the expansion of the cloud after the trapping potential is removed [19]. Since the cloud remains isothermal the Euler equation can be derived using the Gibbs-Duhem relation $dP = nd\mu$. This implies that the equation of motion is independent of the universal function *f(y)* defined in Eq. 10.4. We get

$$\ddot{b}_i = \frac{\omega_i^2}{(b_x b_y b_z)^{2/3}} \frac{1}{b_i}, \tag{10.19}$$

The total energy of the expanding system is given by the sum of internal energy and kinetic energy,

$$E = E_{int} + E_{kin} = \int d^3x \left(\mathscr{E}(x) + \frac{1}{2} mn\vec{v}^2 \right). \tag{10.20}$$

For the Fermi gas at unitarity the energy density $\mathscr{E}$ is related to the pressure by $\mathscr{E} = \frac{3}{2} P$. We find

$$E = E_{int}(0) \left\{ \frac{1}{(b_x b_y b_z)^{2/3}} + \frac{1}{3} \left(\frac{\dot{b}_x^2}{\omega_x^2} + \frac{\dot{b}_y^2}{\omega_y^2} + \frac{\dot{b}_z^2}{\omega_z^2} \right) \right\}, \tag{10.21}$$

where $E_{int}(0)$ is the internal energy at $t = 0$. Conservation of energy immediately follows from the equation of motion, Eq. 10.19. We note that the equation of hydrostatic equilibrium, $\vec{\nabla} P = -n\vec{\nabla} V$, implies the Virial theorem $\langle \mathscr{E} \rangle = \langle V \rangle$ [20], where $\langle V \rangle$ denotes the integral of the potential energy over the trap. This means that the total energy of the trapped gas is $E_0 = 2E_{int}(0)$, where the factor 2 is due to the contribution of the potential energy.

We are interested in an axially symmetric trap with $\omega_y = \omega_z = \omega_\perp$ and $\omega_x = \lambda \omega_\perp$. In this case we end up with two coupled equations for $b_\perp$ and b_x. If $\lambda \gg 1$ the evolution in the transverse direction is much faster and the equation for $b_\perp$ can be approximately decoupled,

$$\ddot{b}_\perp = \frac{\omega_\perp^2}{b_\perp^{7/3}}. \tag{10.22}$$

This equation has to be integrated numerically. The behavior at early and late times can be found analytically. We get

$$b_\perp(t) \simeq \begin{cases} 1 + \frac{1}{2}\omega_\perp^2 t^2 + O(t^4) & \omega_\perp t \ll 1, \\ \frac{\omega_\perp t}{\sqrt{\gamma}} + c_0 + O(t^{-1/3}) & \omega_\perp t \gg 1, \end{cases} , \tag{10.23}$$

where $\gamma = 2/3$ and c_0 is a constant that can be determined by matching the early and late time behavior. Numerically, we find $c_0 \simeq -1.3$. For the longitudinal expansion the early time behavior is $b_x(t) \simeq 1 + (\lambda\omega_\perp t)^2/2$, and at late times $b_x(t) \simeq const \cdot \lambda^2\omega_\perp t$.

The signature effect of hydrodynamics is that transverse pressure gradients cause the transverse radius to expand much faster than the longitudinal radius. This means that the two radii will eventually cross. This happens at a time

$$t_{cross} = \frac{\sqrt{\gamma}}{\omega_x}\left(1 + O(\lambda)\right). \tag{10.24}$$

We note that the crossing time only depends on the trap parameters, and is independent of the initial energy or the number of particles. We also note that at $t \simeq t_{cross}$ the expansion is still two-dimensional, that means the volume of the system grows as $vol \sim t^2$. The expansion becomes three-dimensional, $vol \sim t^3$, at $t_{3d} \sim (\lambda^2\omega_\perp)^{-1}$.

10.3.1 Energy Dissipation

We wish to understand how the expansion is affected by dissipation. The energy momentum tensor of a dissipative fluid is $\Pi_{ij} = P\delta_{ij} + mnv_iv_j + \delta\Pi_{ij}$ with

$$\delta\Pi_{ij} = \eta\left(\nabla_i v_j + \nabla_j v_i - \frac{2}{3}\delta_{ij}\nabla\cdot v\right) + \zeta\delta_{ij}\left(\nabla\cdot v\right). \tag{10.25}$$

The energy current is $j_i^\varepsilon = v_i(w + \frac{1}{2}mnv^2) + \delta j_i^\varepsilon$ with $w = \mathscr{E} + P$ and $\delta j_i^\varepsilon = \delta\Pi_{ij}v_j - \kappa\nabla_i T$. The unitary gas is scale invariant and $\zeta = 0$ [21]. Also, for an isentropic scaling expansion the temperature remains independent of position, and there is no contribution from the thermal conductivity κ. We will therefore concentrate on the role of shear viscosity.

Since the shear viscosity is small, we can take it into account perturbatively. The simplest idea it compute the amount of kinetic energy that is converted to heat. We have

$$\dot{E} = -\frac{1}{2}\int d^3x\,\eta\left(\nabla_i v_j + \nabla_j v_i - \frac{2}{3}\delta_{ij}\nabla\cdot v\right)^2. \tag{10.26}$$

For the scaling expansion given in Eq. 10.10 the result is particularly simple. We get

$$\dot{E} = -\frac{4}{3}\left(\frac{\dot{b}_\perp}{b_\perp} - \frac{\dot{b}_x}{b_x}\right)^2 \int d^3x \eta(x). \tag{10.27}$$

The total energy dissipated is given by the integral of Eq. 10.27 over time. We first show that the spatial integral over $\eta(x)$ does not depend on time. In the local density approximation $\eta(x) = \eta(\mu(x), T)$. Scale invariance implies that

$$\eta(\mu, T) = n(\mu, T)\alpha_n\left(\frac{T}{\mu}\right), \tag{10.28}$$

where $\alpha_n(z)$ is a universal function, and we have set $\hbar = 1$. In order to compare with the string theory bound it is also useful to define $\eta(\mu, T) = s(\mu, T)\alpha_s(T/\mu)$, where we have also set $k_B = 1$. We can write

$$\int d^3x \eta(x) = N\langle\alpha_n\rangle, \tag{10.29}$$

where

$$\langle\alpha_n\rangle = \frac{1}{N}\int d^3x n(x,t)\alpha_n\left(\frac{T(t)}{\mu(x,t)}\right) = \frac{1}{N}\int d^3x n_0(x)\alpha_n\left(\frac{T_0}{\mu(x,0)}\right) \tag{10.30}$$

is an average of α_n over the initial density distribution. Analogously, we can write the integral over $\eta(x)$ as $S\langle\alpha_s\rangle$, where S is the total entropy and $\langle\alpha_s\rangle$ is an average of α_s over the initial entropy density.

The time integral over $(\dot{b}_\perp/b_\perp - \dot{b}_x/b_x)^2$ is dominated by the regime $\omega_\perp t \sim 1$ and converges rapidly – the integral reaches 80% of its asymptotic value at $t_{diss} \simeq 5.9\omega_\perp^{-1}$. In the limit $\lambda \ll 1$ we can neglect the contribution from $\dot{b}_x$. On dimensional grounds the integral over $(\dot{b}_\perp/b_\perp)^2$ must be proportional to $\omega_\perp$. The constant of proportionality can be determined numerically. We find

$$\int_0^\infty dt \left(\frac{\dot{b}_\perp}{b_\perp}\right)^2 = 0.87\omega_\perp. \tag{10.31}$$

We can now compute the ratio $\Delta E/E_{int}$ of the dissipated energy to the initial internal energy of the system. In order to express the result in terms of experimentally measured quantities it is useful to introduce the energy $E_F = N\varepsilon_F$ where $\varepsilon_F = \bar{\omega}(3N)^{1/3}$ is the Fermi energy of the trapped gas and $\bar{\omega} = (\omega_x\omega_y\omega_z)^{1/3}$. We find

$$\frac{\Delta E}{E_{int}(0)} = -\frac{8}{3}\cdot 0.87\cdot\beta = -2.32\cdot\beta \tag{10.32}$$

where the parameter β is defined given by

$$\beta = \frac{\langle\alpha_n\rangle}{(3N\lambda)^{1/3}}\frac{1}{(E_0/E_F)} = \frac{\langle\alpha_s\rangle}{(3N\lambda)^{1/3}}\frac{(S/N)}{(E_0/E_F)}. \tag{10.33}$$

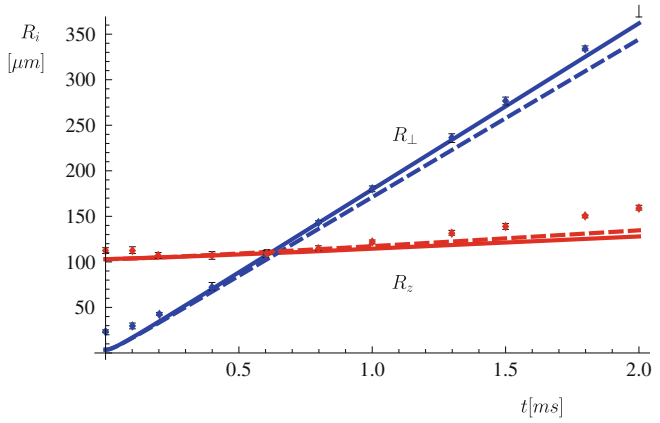

Fig. 10.1 Expansion of the transverse and longitudinal radii after release from a harmonic trap. The data points are taken from [7]. The *solid* and *dashed lines* correspond to solutions of the Navier–Stokes equation with $\langle \alpha_s \rangle = 0$ (*solid lines*) and $\langle \alpha_s \rangle = 0.5$ (*dashed lines*)

Dissipation slows down the transverse expansion of the system. For $(\omega_\perp t) \gg 1$ we have $(\delta \dot{b}_\perp / \dot{b}_\perp) = (\Delta E/E)/2$ and, up to terms that are higher order in λ, the change in the crossing time is directly related to the change in the expansion rate, $(\delta t/t)_{cross} = (\delta \dot{b}_\perp / \dot{b}_\perp)$.

The thermodynamic quantities S/N and E_0/E_F as a function of T/T_F were determined experimentally in [22]. Just above the critical temperature $S/N \simeq 2.2$ and $E_0/E_F \simeq 0.83$. The double ratio $[(S/N)/(E_0/E_F)]$ is only weakly dependent on T, changing by less than 15% between T_c and $4T_c$. In the flow experiment carried out by O'Hara et al. [7] the cloud contained $N = 2 \cdot 10^5$ atoms and the asymmetry parameter was $\lambda = 0.045$. The predicted sensitivity of the crossing time to dissipative effects is

$$\left(\frac{\delta t}{t}\right)_{cross} = 0.008 \left(\frac{\langle \alpha_s \rangle}{1/(4\pi)}\right) \left(\frac{2 \cdot 10^5}{N}\right)^{1/3} \left(\frac{0.045}{\lambda}\right)^{1/3} \left(\frac{S/N}{2.2}\right) \left(\frac{0.83}{E_0/E_F}\right). \tag{10.34}$$

For $\langle \alpha_s \rangle = 1/(4\pi)$ this is at the limit of what can be resolved experimentally, but for $\langle \alpha_s \rangle = 0.5$ the effect reaches about 5%. An example is shown in Fig. 10.1. The solid lines show the solution of the Euler equation (10.19), and the dashed lines show a solution of the Navier–Stokes equation (see Sect. 10.3.2) with $\langle \alpha_s \rangle = 0.5$. The main effect of shear viscosity is a suppression of the transverse expansion of the system. We find $(\delta t/t)_{cross} = 6.5\%$, in fairly good agreement with the estimate $(\delta t/t)_{cross} = 5\%$ from Eq. 10.34.

The best fit to the data is provided by ideal hydrodynamics with $\langle \alpha_s \rangle = 0$. This is probably related to the fact that the data were taken significantly below T_c, at $T/T_F = 0.13 \pm 0.05$. In this regime the system is described by two-fluid hydrodynamics. The superfluid component has no shear viscosity but the viscosity of

the normal component becomes very large as $T/T_F \to 0$ [23]. In a finite system, however, the large viscosity of the normal phase is likely to be suppressed by relaxation time effects, see Sect. 10.3.5. As a consequence one observes perfect superfluid hydrodynamics. The data in Fig. 10.1 show some deviations from hydrodynamics at very early and very late times. Discrepancies at early times are probably related to experimental resolution [7], while the differences at late times may be connected to the breakdown of hydrodynamics in the late stages of the expansion.

We can also compute the amount of entropy generated by dissipative effects. Using $dS = dQ/T$ we find

$$\frac{\Delta S}{N} = \frac{4}{3}\frac{\langle \alpha_n \rangle}{(3N\lambda)^{1/3}}\frac{1}{(T_0/T_F)} I_S \tag{10.35}$$

with

$$I_S = \omega_\perp^{-1} \int_0^\tau dt b_\perp^{-2/3} \left(\dot{b}_\perp\right)^2 . \tag{10.36}$$

For $\tau \simeq t_{diss}$ we find $I_s \simeq 2.6$ and the produced entropy is small, $(\Delta S/N) \simeq 0.27$ for the conditions given above. However, the integral diverges as $I_s \sim (\omega_\perp \tau)^{1/3}$ for $\tau \to \infty$. This result is not reliable since we expect hydrodynamics to break down at late times, see Sect. 10.3.4.

10.3.2 Moments of the Navier–Stokes Equation

It is clearly desirable to study the role of dissipation more directly by solving the Navier–Stokes equation. The Navier–Stokes equation differs from the Euler equation by an extra term on the right hand side,

$$mn\left(\frac{\partial v_i}{\partial t} + \left(\vec{v}\cdot\vec{\nabla}\right)v_i\right) = -\nabla_i P - \nabla_j \delta\Pi_{ij}. \tag{10.37}$$

We will assume that the viscosity is small, so that derivatives with respect to thermodynamic variables can be computed at constant entropy. We will also assume that the entropy conservation equation, Eq. 10.18, is not modified. Physically, this implies that we assume that there is a reservoir that removes the heat generated by dissipative effects. In this case, the only correction to the equations of hydrodynamics is the viscous force in the Navier–Stokes equation.

In general the inclusion of the Navier–Stokes term will break the simple scaling form of the flow. The Navier–Stokes equation also depends on the functional form of the pressure and the viscosity, that means we have to specify the functions $f(y)$ in Eq. 10.4 and $\alpha_n(z)$ in Eq. 10.28. A simple approach that avoids extensive numerical work as well as model assumptions about $f(y)$ and $\alpha_n(z)$ is to take moments of the Navier–Stokes equation. Consider the linear moments

$$m\int d^3x x_k n(x)\left(\frac{\partial v_i}{\partial t}+\left(\vec{v}\cdot\vec{\nabla}\right)v_i\right)=-\int d^3x x_k\Big(\nabla_i P+\nabla_j\delta\Pi_{ij}\Big),\quad (10.38)$$

with $k=1,2,3$. Since the velocity field is linear in the coordinates we find that the ideal fluid terms involve second moments of the density. These moments are related to the potential energy in a harmonic trap and, by the virial theorem, to the total energy of the system. The Navier–Stokes term can be integrated by parts and is proportional to the integral over $\eta(x)$. As a consequence, the first moment of the Navier–Stokes equation depends only on the parameter β defined in Eq. 10.33. We get

$$\ddot{b}_\perp=\frac{\omega_\perp^2}{(b_\perp^2 b_x)^{2/3}b_\perp}-\frac{2\beta\omega_\perp}{b_\perp}\left(\frac{\dot{b}_\perp}{b_\perp}-\frac{\dot{b}_x}{b_x}\right)\quad (10.39)$$

$$\ddot{b}_x=\frac{\omega_x^2}{(b_\perp^2 b_x)^{2/3}b_x}+\frac{4\beta\lambda\omega_x}{b_x}\left(\frac{\dot{b}_\perp}{b_\perp}-\frac{\dot{b}_x}{b_x}\right).\quad (10.40)$$

These equations of motion are consistent with the result in the previous section. We can compute the amount of energy dissipated from Eqs. 10.21 and (10.39, 10.40). We find

$$\dot{E}=-\frac{8}{3}\beta E_{int}(0)\left(\frac{\dot{b}_\perp}{b_\perp}-\frac{\dot{b}_x}{b_x}\right)^2.\quad (10.41)$$

We note that $b_\perp(t)$ and $b_z(t)$ are solutions of the Navier–Stokes equation and have an implicit dependence on β. As long as this dependence is smooth, $b_i(t,\beta)\to b_i(t,0)$ as $\beta\to 0$, Eq. 10.41 reduces to Eq. 10.27 at leading order in β. Since typical values of β are quite small, we expect the estimates in the previous section to be very accurate. This is studied in more detail in Fig. 10.2. We observe that the dissipated energy $(\Delta E)/E$ is very linear in β even for values of $(\Delta E)/E$ as large as 25%. We note that because of turbulence solutions of the Navier–Stokes equation do not in general approach solutions of the Euler equation in the limit that the shear viscosity goes to zero. Turbulence is not present in our analysis because we do not consider small fluctuations. We also note that there is no continuous forcing in the case of an expanding gas and it is not clear whether turbulence can develop even if fluctuations are included. We will estimate the Reynolds number of the flow in Sect. 10.3.4.

10.3.3 Scaling Solution of the Navier–Stokes Equation

In this section we discuss a specific model for the density dependence of the shear viscosity that preserves the scaling nature of the flow even if the viscosity is not zero. This model allows to compute the local amount of heat that is generated by

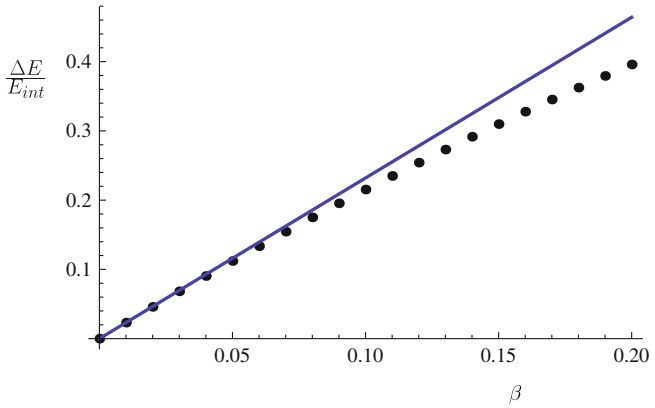

Fig. 10.2 This figure show the ratio $(\Delta E)/E_{int}$ of the dissipated energy to the initial internal energy as a function of the parameter β defined in Eq. 10.33. The dots show the result of a numerical solution of the Navier–Stokes equation (10.39, 10.40) in the limit $\omega_z/\omega_\perp \to 0$ and the line shows the estimate given in Eq. 10.32

dissipation, and to understand some of the shortcomings of the method discussed in Sects. 10.3.1 and 10.3.2. Consider

$$\eta(n,T) = \eta_0 (mT)^{3/2} + \eta_1 \frac{P(n,T)}{T}, \tag{10.42}$$

where $\eta_{0,1}$ are constants and *P(n,T)* is the pressure. The first term dominates in the low density, high temperature limit. This is the regime in which a kinetic description in terms of weakly coupled atoms is applicable. Kinetic theory gives [24, 25]

$$\eta_0 = \frac{15}{32\sqrt{\pi}}. \tag{10.43}$$

The second term dominates in the high density, low temperature regime. The functional form of this term is not motivated by kinetic theory. We note, however, that η/n has a minimum as a function of T, as expected on theoretical [23] and phenomenological grounds [3].

The model given in Eq. 10.42 has two remarkable features: first, the η_0 term does not contribute to the Navier–Stokes equation at all. The Navier–Stokes term $\nabla_j[\eta_0(mT)^{3/2}(\nabla_i v_j + \cdots)]$ vanishes since both T and $\nabla_i v_j$ are constant. Second, the η_1 term preserves the scaling flow. Using $T, \nabla_i v_j \sim const$ we see that $\nabla_j[\eta_1 P(n,T)/T(\nabla_i v_j + \cdots)]$ scales like the contribution from the pressure of an ideal fluid, $\nabla_i P(n,T)$. We get

$$\ddot{b}_\perp = \frac{\omega_\perp^2}{(b_\perp^2 b_x)^{2/3} b_\perp} - \frac{2\eta_1 \omega_\perp^2}{3T_0 b_\perp}\left(\frac{\dot{b}_\perp}{b_\perp} - \frac{\dot{b}_x}{b_x}\right) \tag{10.44}$$

$$\ddot{b}_x = \frac{\omega_x^2}{(b_\perp^2 b_x)^{2/3} b_x} + \frac{4\eta_1 \omega_x^2}{3T_0 b_x}\left(\frac{\dot{b}_\perp}{b_\perp} - \frac{\dot{b}_x}{b_x}\right). \tag{10.45}$$

We observe that these equations are identical to the moment Eqs. 10.39, 10.40 with $\beta = \eta_1 \omega_\perp/(3T_0)$. This is not a surprise – the η_1 contribution to $\eta(n, T)$ vanishes as $n \to 0$ and the assumptions underlying the moment method are satisfied. The η_0 term, on the other hand, does not vanish as $n \to 0$, and it cannot be included in the moment equations (it makes an infinite contribution to the integral over $\eta(x)$).

Using the identification $\beta = \eta_1 \omega_\perp/(3T_0)$ we can write

$$\beta = \frac{\eta_1}{3(3\lambda N)^{1/3}} \frac{1}{(T_0/T_F)}, \tag{10.46}$$

which shows that any bound on $\langle \alpha_n \rangle$ obtained using the methods of Sect. 10.3.2 can be translated into an estimate of η_1, $\eta_1 = 3(T_0/E_0)\langle \alpha_n \rangle$. Near T_c this implies that $\eta_1 \simeq 0.76 \langle \alpha_n \rangle$. We note that the relation between η_1 and $\langle \alpha_n \rangle$ is precisely what one obtains if the trap average of $\eta(x)$ is computed from the η_1-term only. The situation is more complicated if the contribution from η_0 is taken into account. The ratio η/n is given by

$$\frac{\eta(n, T)}{n} = \eta_0 y^{3/2} + \frac{\eta_1}{y} f(y) \tag{10.47}$$

with $y = (mT)/n^{2/3}$. Since $f(0) = const$ and $f(y) \simeq y$ for $y \gg 1$ this function has a minimum, see Fig. 10.3. The figure also shows that $(\eta/n)_{min}$ receives significant contributions from η_0. It is clearly unsatisfactory that our analysis has no sensitivity to this term. We will return to this issue in Sect. 10.3.5.

Using the explicit form of $\eta(n, T)$ we can also address the question where the energy is being dissipated and how much reheating is taking place. We first consider the contribution from η_1. The energy dissipated is

$$\dot{\mathscr{E}} = -\frac{4\eta_1}{3}\left(\frac{\dot{b}_\perp}{b_\perp}\right)^2 \frac{P(n, T)}{T}. \tag{10.48}$$

For a Fermi gas at unitarity the energy density is related to the pressure by $\mathscr{E}(n, T) = (3/2)P(n, T)$. Equation (10.48) implies that the energy dissipated is proportional to the local internal energy density. The source of the dissipated energy is the reduction in the kinetic energy density relative to its value in ideal hydrodynamics. The local kinetic energy density is

$$\mathscr{E}_{kin} = \frac{m}{2} n \left(\frac{\dot{b}_\perp}{b_\perp}\right)^2 x_\perp^2. \tag{10.49}$$

Since the kinetic energy density differs from the spatial distribution of the dissipated energy there has to be a dissipative contribution to the energy current. This current is given by $\delta \vec{j}^{\,\varepsilon} = (0, \delta j_y^\varepsilon, \delta j_z^\varepsilon)$ with

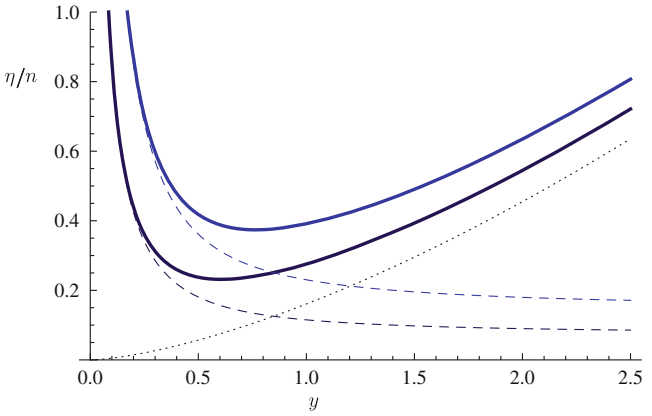

Fig. 10.3 Ratio η/n as a function of $y = (mT)/n^{2/3}$ for the model defined in Eq. 10.42. The two curves correspond to (from *bottom* to *top*) $\eta_1 = 1/(4\pi), 2/(4\pi)$ with $\eta_0 = 15/(32\sqrt{\pi})$. The *dashed line* shows the contribution from η_1, which is the term that contributes directly to the Navier–Stokes equation, and the *dotted line* is the contribution from η_0. Note that the critical point for the onset of superfluidity is $y_c \simeq 0.72$

$$\delta j_z^{\varepsilon} = v_z \delta \Pi_{zz} = -z \frac{2\eta_1 P(n,T)}{3T} \left(\frac{\dot{b}_\perp}{b_\perp}\right)^2, \tag{10.50}$$

and $\delta j_y^{\varepsilon} = \delta j_z^{\varepsilon}(z \leftrightarrow y)$. The dissipative current flows from the outer edge of the cloud, where the kinetic energy is peaked, to the center of the cloud, where the pressure is largest.

Energy dissipation leads to reheating. The change in temperature is $\Delta T = (\Delta \mathscr{E})/c_V$. The time evolution of the temperature is governed by

$$\dot{T} = -\frac{4T_0}{3b_\perp^{4/3}} \left(\frac{\dot{b}_\perp}{b_\perp}\right) + \frac{\eta_1 P}{c_V T} \left(\frac{\dot{b}_\perp}{b_\perp}\right)^2, \tag{10.51}$$

where the first term is related to the adiabatic expansion of the system, and the second term is the dissipative correction. Note that if $c_V \sim \mathscr{E}/T$, which is the case in the high temperature limit, then reheating will preserve the fact that the cloud is isothermal. In general the behavior of the specific heat is more complicated and dissipation produces a temperature gradient. The relative importance of reheating is governed by the parameter $(\eta_1 \omega_\perp / T_0)(P/(c_V T))$. In the high temperature limit we can use $P \sim c_V T$ and this expression reduces to the parameter β defined in Eq. 10.46. Reheating becomes important at a time $\omega_\perp t \sim \beta^{-3}$. Since β is typically very small, this occurs very late during the evolution of the system.

A similar analysis of the effects of η_0 leads to a number of puzzles. The energy dissipated is independent of density, and the total energy dissipated over all space is infinite. There is no change in the kinetic energy, and the source of the dissipated energy is the viscous correction to the energy current. This current flows into the

system from spatial infinity. The relative importance of reheating is governed by the parameter $(\eta_0\omega_\perp/T_0)((mT)^{3/2}/n)$, which is always large in the dilute region of the cloud.

10.3.4 Breakdown of Hydrodynamics

The constant term $\eta \sim \eta_0(mT)^{3/2}$ in the shear viscosity dominates in the dilute outer regions of the cloud, and the difficulty in understanding the effects of this term must be related to the breakdown of hydrodynamics in the dilute regime. A standard criterion for the applicability of hydrodynamics is the condition that the Knudsen number $Kn = l_{mfp}/L$, the ratio of the mean free path to the system size, is much less than one. In the dilute regime the mean free path is given by

$$l_{mfp} = \frac{1}{n\sigma} = \frac{3}{4\pi}\frac{mT}{n}. \tag{10.52}$$

The density is given by Eq. 10.6. In the dilute regime we can use the high temperature limit of *h(z)*, but the scaling arguments in the following are independent of the functional form of *h(z)*. For a comoving observer the density scales as $n \sim (m\mu)^{3/2}$, and the mean free path scales as $l_{mfp} \sim T/(m^{1/2}\mu^{3/2})$. The evolution of T and μ is governed by the scaling relations discussed in Sect. 10.2. We may use, in particular, that $T/\mu \sim const$ and $\mu \sim \mu(0)/(b_\perp^2 b_x)^{2/3}$. We conclude that in a comoving fluid cell

$$Kn = \frac{l_{mfp}}{L} \sim \left(\frac{b_x}{b_\perp}\right)^{1/3}. \tag{10.53}$$

During the two-dimensional expansion the Knudsen number is dropping, which implies that the hydrodynamic description is becoming more accurate. In the late, three-dimensional stage, the Knudsen number is constant.

A more accurate criterion can be obtained by using a characteristic length or time scale derived from the flow profile. Hydrodynamics is based on a derivative expansion of the energy momentum tensor, and the validity of hydrodynamics requires that $\delta\Pi_{ij}$ is small compared to the ideal fluid stress tensor. Consider the ratio of the moments of the ideal and dissipative terms on the RHS of the Navier–Stokes equation

$$\frac{\langle x_k \nabla_k P\rangle}{\langle x_k \nabla_j \delta\Pi_{kj}\rangle} = \frac{\langle P\rangle}{\langle \frac{4}{3}\eta(\nabla_k v_k)\rangle} \tag{10.54}$$

where $\langle . \rangle$ denotes an integral over d^3x and the index k is fixed. The ratio $(\eta/P)(\nabla\cdot v)$ has a simple interpretation in kinetic theory. For a dilute gas $\eta \sim npl_{mfp} \sim \rho u^2 \tau_{mft}$ and $P \sim \rho u^2$, where n is the particle density, ρ is the mass density, p is the average quasi-particle momentum, u the average velocity, and τ_{mft} the mean free time. The ratio $\nabla \cdot v \sim \tau_{exp}^{-1}$ defines a characteristic expansion time. The quantity

$$\frac{\eta}{P}(\nabla \cdot v) \sim \frac{\tau_{mft}}{\tau_{exp}} \tag{10.55}$$

measures the ratio of the mean free time over the expansion time. Hydrodynamics is valid if $\tau_{mft} \ll \tau_{exp}$. We observe that for $\eta \sim P$ the freezeout criterion is independent of position and only a function of time. We get

$$\frac{\eta}{P}(\nabla_z v_z) = \frac{\eta_1}{T_0}\,(b_x b_\perp)^{1/3}\,\dot{b}_\perp \simeq \frac{\eta_1}{(3N)^{1/3}\lambda^{1/3}}\,\frac{1}{(T_0/T_F)}\,(\omega_\perp t)^{1/3}\,, \tag{10.56}$$

where we have assumed that the expansion is two-dimensional. We note that the relevant parameter is the quantity β defined in Eq. 10.46. Freezeout occurs at $(\omega_\perp t_{fr}) \sim \beta^{-3}$. For typical values of β we find that $t_{fr} \gg t_{cross} \gg t_{diss}$, where $t_{cross} \sim (\omega_\perp \lambda)^{-1}$ is the crossing time, and $t_{diss} \sim 5.9\omega_\perp^{-1}$ is the characteristic time for dissipative effects.

The freezeout time defined by Eq. 10.56 is very long, and the physical freezeout is determined by the viscous effects in the dilute part of the cloud. In the case of a spatially constant shear viscosity we find

$$\frac{\eta}{P}(\nabla_z v_z) = \frac{\eta_0 (mT)^{3/2}}{P}\left(\frac{\dot{b}_\perp}{b_\perp}\right) \simeq \frac{45\pi}{8\sqrt{2}}\,\frac{(T_0/T_F)^2}{(3\lambda N)^{1/3}}\,b_\perp^{1/3}\dot{b}_\perp \exp\left(\sum_i \frac{x_i^2}{b_i^2 \bar{R}_i^2}\right), \tag{10.57}$$

where we have used $P = nT$ as well as the low density (high temperature) limit of $n_0(x)$, see Eq. 10.6. The radius parameter $\bar{R}_i$ is defined as $\bar{R}_i^2 = 2T_0/(m\omega_i^2)$. The condition $(\eta/P)(\nabla_z v_z)$ determines a freezeout surface $x_{fr}(t)$. This surface is initially at $x_i \gg R_i$, but it moves inward as time increases and reaches the origin at a time $t_{fr} \sim \omega_\perp^{-1}(3\lambda N)(T_F/T_0)^6$. This time is also parametrically very long, but the freezeout time at a characteristic distance $x_i \simeq b_i \bar{R}_i$ is significantly smaller.

Finally, we wish to mention one more quantity that characterizes a viscous flow. The Reynolds number Re is defined as the ratio of inertial and viscous forces in the system. In the case of a scaling flow with $\eta \sim P$ this ratio is independent of position and only a function of time. We find

$$Re = \frac{T_0}{\eta_1 \omega_\perp^2} b_\perp \dot{b}_\perp \simeq \frac{\omega_\perp t}{\beta}. \tag{10.58}$$

The Reynolds number is zero initially, but it grows quickly, reaching $Re \simeq \beta^{-1}$ at $(\omega_\perp t) = 1$. For typical experimental parameters $\beta^{-1} \sim 100$, which is large but not large enough to cause instabilities. At later times even larger values of Re are reached, but at these late times the system is simply free streaming. A constant contribution to the viscosity does not lead to a viscous force, and does not directly contribute to the Reynolds number.

10.3.5 Relaxation Time Approach

The discussion in the previous section does not fully resolve the problems caused by the dilute regions of the cloud. If the shear viscosity is proportional to the pressure then the system freezes out at some time t_{fr}. For values of η/P implied by the data this time is much larger than the characteristic time for dissipative effects in the evolution of the system, and the estimates in Sects. 10.3.1–10.3.3 are internally consistent. If the shear viscosity is constant then there is a freezeout surface which moves inward as a function of time. This implies that the integral in Eqs. 10.27 and 10.38 should be restricted to the region enclosed by the freezeout surface. However, in order for energy to be conserved, and for viscosity to have an effect on the evolution of the system, we would have to include an external force on the freezeout surface.

An approach that can describe the effects of freezeout without the need to introduce an artificial surface is second order viscous hydrodynamic [26]. The second order formalism takes into account terms with two derivatives of the thermodynamic variables in the dissipative correction to the stress tensor and energy current. In general, the second order formalism contains a large number of new transport coefficients. A phenomenological ansatz that has proven to be useful in many different applications is to treat the viscous part of the stress tensor as an independent hydrodynamical variable which satisfies a relaxation equation

$$\tau_R \frac{\partial}{\partial t} \delta\Pi_{ij} = -\delta\Pi_{ij} + \delta\Pi_{ij}^{NS}, \tag{10.59}$$

where τ_R is the relaxation time and $\delta\Pi_{ij}^{NS}$ is the Navier–Stokes expression for the viscous contribution to the stress tensor, Eq. 10.25. An equation of this type was first introduced by Maxwell and Cattaneo in the context of heat transport. More recently, time or frequency dependent viscosities were considered in the study of Bose condensed gases in [27, 28]. In relativistic hydrodynamics relaxation equations for the viscous stress tensor are used in order to restore causality, see the review [29].

Scale invariance implies that $\tau_R(n, T) = w(mT/n^{2/3})/T$ where $w(y)$ is a universal function. In the dilute limit $y \gg 1$ the function $w(y)$ can be calculated in kinetic theory which gives $\tau_R = \eta/(nT)$ [30]. This result corresponds to the estimate for τ_{mft} given in Eq. 10.55. The relaxation equation (10.59) requires an initial condition for the viscous stress $\delta\Pi_{ij}$. If is natural to assume that $\delta\Pi_{ij} = 0$ at $t = 0$. In the center of the cloud τ_R is small and the viscous stress quickly relaxes to the Navier–Stokes result. In the dilute region $\tau_R \to \infty$ and the viscous contribution to the stress tensor remains zero. This implies that even a spatially constant shear viscosity leads to a spatially varying $\delta\Pi_{ij}$ and a non-zero drag force. This drag force is largest near the freezeout surface and breaks the scaling nature of the flow. This means that a detailed study of the Israel-Stewart equations will require numerical solutions of the hydrodynamic equations. We can estimate the effect of the relaxation time by computing the energy dissipation. We have

$$\dot{E} = -\frac{1}{2} \int d^3x \delta\Pi_{ij} \left(\nabla_i v_j + \nabla_j v_i - \frac{2}{3} \delta_{ij} \nabla \cdot v \right), \tag{10.60}$$

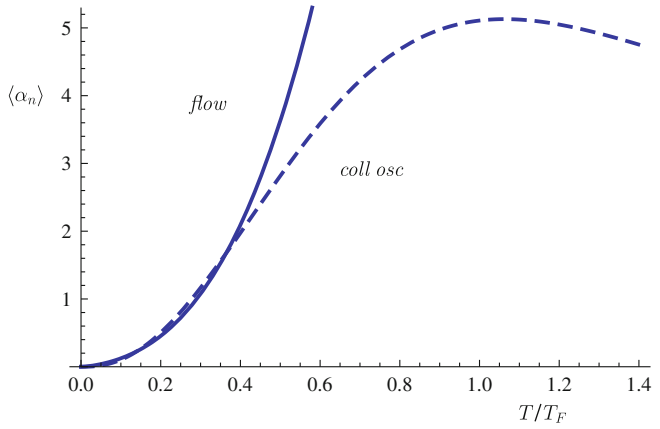

Fig. 10.4 Trap average $\langle\alpha_n\rangle = \langle\eta\rangle/N$ computed from a relaxation time equation with $\eta = \eta_0(mT)^{3/2}$ and $\tau_R = \eta/(nT)$. Contrary to the pure Navier–Stokes case $\tau_R \to 0$ the ratio $\langle\eta\rangle/N$ depends on the number of particles and the trap geometry. Here we have chosen $N = 2 \cdot 10^5$ and $\lambda = 0.045$. The *solid* shows the result for the elliptic flow field, and the *dashed line* corresponds to the transverse collective mode, see Sect. 10.5

where $\delta\Pi_{ij}$ is determined by Eq. 10.59. The simplest approximation is to set $\delta\Pi_{ij} = \delta\Pi_{ij}^{NS}$ inside the freezeout surface and $\delta\Pi_{ij} = 0$ outside.

In order to obtain more accurate estimates we have to solve the differential equation (10.59). As in Sect. 10.3.1 we may compute $\delta\Pi_{ij}^{NS}$ from the solution of ideal hydrodynamics. The relaxation time can be calculated using the high temperature result for the density profile. We find

$$\omega_\perp \tau_R = \frac{45\pi}{8\sqrt{2}} \frac{1}{(3\lambda N)^{1/3}} \left(\frac{T}{T_F}\right)^2 b_\perp^{4/3} \exp\left(\frac{x_\perp^2}{b_\perp^2 \bar{R}_\perp^2} + \frac{x_z^2}{\bar{R}_z^2}\right), \tag{10.61}$$

which has the same functional form as the freezeout criterion in Eq. 10.57. The viscous stress tensor $\delta\Pi_{ij}$ is determined by integrating Eq. 10.59 and the dissipated energy can be computed from Eq. 10.60. By comparing ΔE with Eq. 10.27 we can express the result in terms of an effective $\langle\alpha_n\rangle$. This quantity is shown in Fig. 10.4. We observe that $\langle\alpha_n\rangle$ grows with temperature as $\langle\alpha_n\rangle \sim T^3$, much faster than one would expect from the relation $\eta \sim T^{3/2}$.

There are no data for elliptic flow at temperatures above T_c, but we will compare the relaxation time result to collective mode data in Sect. 10.5. We note that at low temperature the effective $\langle\alpha_n\rangle$ is the same for expanding and oscillating systems, but that at high temperature the two systems behave differently. In the expanding system the hydrodynamic expansion time τ_{exp} continues to increase during the expansion, whereas the period of the oscillation provides a fixed hydrodynamic time scale in the case of the collective mode. The viscous relaxation time τ_R increases with temperature. This implies that for the collective mode we eventually get $\tau_R > \tau_{exp}$ and the effective $\langle\alpha_n\rangle$ starts to decrease. In the expanding system, on the other hand, the

relaxation time can always match the expansion time and $\langle \alpha_n \rangle$ continues to grow with temperature.

10.4 Expansion From a Rotating Trap

The expansion from a rotating trap was studied in [14]. Rotating gases are of interest for a number of reasons. The quenching of the moment of inertia in a superfluid Bose gas was used as a signature of superfluidity [31]. The remarkable discovery in [14] is that in a Fermi gas at unitarity the suppression of the moment of inertia is also observed in the normal phase. It is clearly of interest to determine to what extent this discovery places constraints on the shear viscosity [32].

10.4.1 Ideal Fluid Dynamics

The Euler equations for a Bose gas with $P \sim n$ were derived in [31]. The result is easily generalized to a Fermi gas at unitarity [14]. As in the case of a non-rotating trap the equations are independent of the temperature and the universal function *f(y)* in Eq. 10.4. We have

$$\dot{\alpha}_x + \alpha_x^2 + \alpha^2 - \Omega^2 = \frac{\bar{\mu}\omega_x^2}{b_x^2} \tag{10.62}$$

$$\dot{\alpha}_y + \alpha_y^2 + \alpha^2 - \Omega^2 = \frac{\bar{\mu}\omega_y^2}{b_y^2} \tag{10.63}$$

$$\dot{\alpha}_z + \alpha_z^2 = \frac{\bar{\mu}\omega_z^2}{b_z^2} \tag{10.64}$$

$$\dot{\alpha} + \alpha\left(\alpha_x + \alpha_y\right) = \frac{\bar{\mu}a\omega_x^2}{2} \tag{10.65}$$

$$\dot{\Omega} + \Omega\left(\alpha_x + \alpha_y\right) = 0. \tag{10.66}$$

These equations have to be solved together with the continuity Eqs. (10.12–10.16). In all there are ten coupled equations. In the case of a rotating trap there is no initial expansion, $\alpha_i(0) = 0$, but either $\alpha(0)$ or $\Omega(0)$ (or both) are non-zero. If the initial flow is purely irrotational then $\alpha(0) = \omega_{rot}$, where ω_{rot} is the angular velocity of the trap. If the flow corresponds to rigid rotation then $\Omega(0) = \omega_{rot}$. Below the critical temperature the flow of the superfluid component must be irrotational, but above T_c both rotational and irrotational flows are possible.

The equations simplify in the experimentally relevant case of strongly deformed, slowly rotating traps, $\omega_{rot} < \omega_x \ll \omega_\perp$ with $\omega_\perp = \omega_y \simeq \omega_z$. In this limit the motion of the fluid is dominated by the transverse expansion of the system. Up to corrections of order $O(\lambda^2)$ or $O((\omega_{rot}/\omega_\perp)^2)$ we have

$$b_\perp(t) \simeq \begin{cases} 1 + \frac{1}{2}\omega_\perp^2 t^2 + O(t^4) & \omega_\perp t \ll 1, \\ \frac{\omega_\perp t}{\sqrt{\gamma}} + c_0 + O(t^{-1/3}) & \omega_\perp t \gg 1, \end{cases} \tag{10.67}$$

as in the case of a stationary trap. The orientation of the expanding cloud is described by the parameter a defined in Eq. 10.11. We find

$$a(t) \simeq \begin{cases} -\frac{2\omega_{rot} t}{\lambda^2} & \omega_\perp t \ll 1, \\ -\frac{c_a \omega_{rot}}{\lambda^2 \omega_\perp^2 t} & \omega_\perp t \gg 1 \ (t < t_{3d}), \end{cases} \tag{10.68}$$

where c_a is a constant. Below we will show that $c_a = \gamma$. At very late times, $t > t_{3d} \sim 1/(\lambda^2 \omega_\perp)$, we find $a(t) \sim 1/t^2$. The result (10.68) holds irrespective of the nature of the initial rotational flow. The parameter *a(t)* can be related to the angle of the cloud with respect to the x-axis,

$$\tan(2\theta) = -\frac{a\lambda^2 b_x^2 b_y^2}{b_x^2 - \lambda^2 b_y^2}. \tag{10.69}$$

At early times, $\omega_x t \ll 1$, the angle is proportional to the rotational frequency of the trap, $\theta = \omega_{rot} t$. The angular motion speeds up as $b_y \lambda$ approaches b_x. The angle goes through 45° at

$$t_{45^\circ} = \frac{\sqrt{\gamma}}{\omega_x} \tag{10.70}$$

which is the identical to the crossing time in Eq. 10.24. At late times, and up to corrections of $O(\omega_{rot}/\omega_\perp)$, the angle approaches 90°. The velocity field is dominated by the transverse expansion of the system. In the limit $\omega_{rot} < \omega_x \ll \omega_\perp$ the velocity fields α_i are identical to those in the non-rotating case. We have

$$\alpha_{y,z} \simeq \begin{cases} \omega_\perp^2 t & \omega_\perp t \ll 1, \\ 1/t & \omega_\perp t \gg 1, \end{cases} \tag{10.71}$$

and $\alpha_x = O(\lambda^2)$. The rotational components of the velocity field decay quickly. If the initial flow is irrotational, $\alpha(0) = \omega_{rot}$, then

$$\alpha(t) \simeq \omega_{rot} \left(1 - \omega_\perp^2 t^2\right) \tag{10.72}$$

for $(\omega_\perp t) < 1$. For $(\omega_\perp t) > 1$ the rotational component of the flow is small, $(\alpha/\omega_{rot}) \ll 1$, but the remaining flow decays slowly, $\alpha \sim t^{-1}$ for $t < t_{3d}$ and $\alpha \sim t^{-2}$

for $t > t_{3d}$. In ideal hydrodynamics an initially irrotational flow will remain irrotational, $\Omega(t) = 0$, for all t. If the initial flow corresponds to rigid rotation, $\Omega(0) = \omega_{rot}$, then the early time behavior is given by

$$\Omega(t) \simeq \omega_{rot}\left(1 - \frac{1}{2}\omega_\perp^2 t^2\right). \tag{10.73}$$

An initially rigid rotating flow induces a non-zero irrotational flow. For $(\omega_\perp t) > 1$ both components of the velocity field become much smaller than ω_{rot}.

The angular momentum is given by

$$L_z = \alpha m\langle n(x^2 - y^2)\rangle + \Omega m\langle n(x^2 + y^2)\rangle + \left(\alpha_x - \alpha_y\right) m\langle nxy\rangle, \tag{10.74}$$

where n is the density and $\langle . \rangle$ is an integral over the cloud. The moment of inertia of a rigid rotor is $I_{rig} = m\langle x^2 + y^2\rangle$, and the irrotational moment of inertia is $I_{irr} = m\langle x^2 - y^2\rangle$. We have

$$m\langle nx^2\rangle = \frac{b_x^2}{1 - \frac{\lambda^2}{4}(ab_xb_y)^2}\frac{L_0}{\omega_x}, \tag{10.75}$$

$$m\langle ny^2\rangle = \frac{\lambda^2 b_y^2}{1 - \frac{\lambda^2}{4}(ab_xb_y)^2}\frac{L_0}{\omega_x}, \tag{10.76}$$

$$m\langle nxy\rangle = \frac{-\frac{\lambda^2}{2}ab_x^2b_y^2}{1 - \frac{\lambda^2}{4}(ab_xb_y)^2}\frac{L_0}{\omega_x}, \tag{10.77}$$

where the scale is set by

$$L_0 = \frac{N}{6}\frac{(3N)^{1/3}}{\lambda^{2/3}}\left(\frac{E_0}{E_F}\right). \tag{10.78}$$

In the experiment of Clancy et al. $(\omega_{rot}/\omega_x) \simeq 0.4$ and $L_0/N \simeq 131(E_0/E_F)$. For $E_0/E_F = 1$, which is in the normal phase, the angular momentum per particle is $50\hbar$.

At early times the trap is strongly deformed and $I_{rig} \simeq I_{irr}$. When the cloud becomes almost spherical the irrotational moment is much smaller than the rigid moment of inertia, $I_{irr} \ll I_{rig}$. However, at times $(\omega_\perp t) > 1$ the angular momentum is mainly carried by the last term in Eq. 10.74, which is related to the transverse expansion of the system. This is true irrespective of the nature of the initial rotational flow. For $(\omega_\perp t) > 1$ we have $\alpha_y m\langle nxy\rangle \simeq (c_a/\gamma)(\omega_{rot}/\omega_x)L_0$. Angular momentum conservation then fixes the constant c_a in Eq. 10.68, $c_a = \gamma$. At very late time, $t > t_{3d}$, the angular momentum is shared among all the terms in Eq. 10.74, and the relative size of the different contributions depends on the initial conditions. In practice, of course, hydrodynamics is no longer applicable at $t > t_{3d}$.

10.4.2 Dissipation

The effects of dissipation on the expansion from a rotating trap can be studied in close analogy with Sects. 10.3.1–10.3.5. The rate of energy dissipation is

$$\dot{E} = -\frac{4}{3}\left(\alpha_x^2+\alpha_y^2+\alpha_z^2-\alpha_x\alpha_y-\alpha_x\alpha_z-\alpha_y\alpha_z+3\alpha^2\right)\int d^3x\,\eta(x). \quad (10.79)$$

For $\alpha_x \simeq \alpha_y \gg \alpha_z, \alpha$ this expression reduces to the energy dissipated by the transverse expansion of cloud, see Eq. 10.27. This implies that the main effect of dissipation is to slow the transverse expansion of the cloud, and to delay the time t_{45°. This delay is exactly the same as the delay in the crossing time in Eq. 10.34. We have

$$\left(\frac{\delta t}{t}\right)_{45^\circ} = 0.009\left(\frac{\langle\alpha_s\rangle}{1/(4\pi)}\right)\left(\frac{1.3\cdot 10^5}{N}\right)^{1/3}\left(\frac{0.3}{\lambda}\right)^{1/3}\left(\frac{S/N}{4.8}\right)\left(\frac{2.1}{E_0/E_F}\right). \quad (10.80)$$

We can confirm this estimate by solving the Navier–Stokes equation. The Navier–Stokes equation can be derived using the moment method described in Sect. 10.3.2. As before, an equivalent set of equations can be obtained from the viscosity model given in Eq. 10.42. We get [33]

$$\dot{\alpha}_x+\alpha_x^2+\alpha^2-\Omega^2 = \frac{\omega_x^2}{b_x^2}\left\{\bar{\mu}-\frac{6\beta}{\omega_\perp}\left[\frac{2}{3}\alpha_x-\frac{1}{3}\left(\alpha_y+\alpha_z\right)+\frac{1}{2}ab_x^2\alpha\right]\right\} \quad (10.81)$$

$$\dot{\alpha}_y+\alpha_y^2+\alpha^2-\Omega^2 = \frac{\omega_y^2}{b_y^2}\left\{\bar{\mu}-\frac{6\beta}{\omega_\perp}\left[\frac{2}{3}\alpha_y-\frac{1}{3}\left(\alpha_x+\alpha_z\right)+\frac{1}{2}a\lambda^2b_y^2\alpha\right]\right\} \quad (10.82)$$

$$\dot{\alpha}_z+\alpha_z^2 = \frac{\omega_z^2}{b_z^2}\left\{\bar{\mu}-\frac{6\beta}{\omega_\perp}\left[\frac{2}{3}\alpha_z-\frac{1}{3}\left(\alpha_x+\alpha_y\right)\right]\right\} \quad (10.83)$$

$$\dot{\alpha}+\alpha\left(\alpha_x+\alpha_y\right) = \omega_x^2\left\{\frac{\bar{\mu}a}{2}-\frac{3\beta}{\omega_\perp}\left[\frac{a}{6}\left(\alpha_x+\alpha_y-2\alpha_z\right)+\frac{b_x^2+\lambda^2b_y^2}{\lambda^2b_x^2b_y^2}\alpha\right]\right\} \quad (10.84)$$

$$\dot{\Omega}+\Omega\left(\alpha_x+\alpha_y\right) = \frac{3\beta\omega_x^2}{\omega_\perp}\left[\frac{a}{2}\left(\alpha_x-\alpha_y\right)+\frac{b_x^2-\lambda^2b_y^2}{\lambda^2b_x^2b_y^2}\alpha\right]. \quad (10.85)$$

These equations are independent of the functional form of the pressure. A solution of the Navier–Stokes equation for the trap parameters and initial conditions in [14] is shown in Fig. 10.5. The experimental data were taken at $E/E_F = 0.56$ which is in the superfluid phase, and $E/E_F = 2.1$ which is significantly above the phase transition. Similar to the low temperature data for pure transverse expansion in Fig. 10.1 the

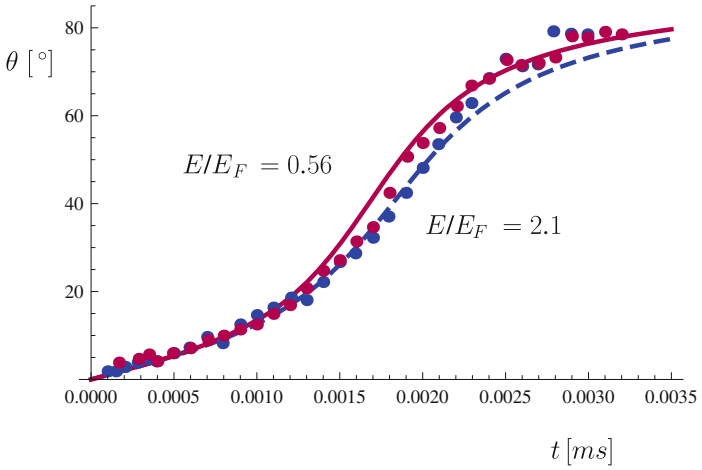

Fig. 10.5 Time evolution of the angle of the major axis of a rotating expanding cloud after release from the trapping potential. The data are taken from [14]. The two data sets were obtained with initial energies $E/E_F = 0.56$ and 2.1. The *solid line* shows the prediction of ideal fluid dynamics, and the *dashed lines* shows the solution of the Navier–Stokes equation for $\beta = 0.061$. Using an entropy per particle $S/N \simeq 4.8$ this value of β implies a shear viscosity to entropy density ratio $\langle \alpha_s \rangle = 0.60$

low temperature result for a rotating cloud shows no dissipative effects, and the best fit to the data is provided by ideal fluid dynamics.

The data for $E/E_F = 2.1$ clearly show a delayed expansion. We find $(\delta t/t)_{45^\circ} \simeq 0.063$. Using $(\delta t/t) \simeq 1.16\beta$ from Eq. 10.32 we estimate $\beta \simeq 0.057$. This estimate is quite accurate, the best fit of the Navier–Stokes solution to the data is obtained for $\beta = 0.061$. Using $N = 1.3 \cdot 10^5$, $\lambda = 0.03$ [14] and $(S/N) \simeq 4.8$ [22] we obtain $\langle \alpha_s \rangle \simeq 0.60$. The measurements were extended to values of E/E_F between 0.56 and 2.1 in [32]. This work reports values of η/s as small as $\langle \alpha_s \rangle \simeq (0.0 - 0.4)$. Note that in this regime it becomes very difficult to measure the viscosity accurately. A value of $\langle \alpha_s \rangle = 0.1$ affects the measured angle of the cloud by less than the with of the lines in Fig. 10.5.

A more detailed study of viscous effects on the evolution of the system is shown in Figs. 10.6, 10.7 10.8. We observe that viscosity slows down the evolution of the scale parameters b_y, b_z and a. More interesting is the effect on the velocity fields α and Ω. Viscosity converts a fraction of the irrotational velocity field α into the rotational velocity field Ω. This is also seen in the breakdown of the angular momentum, see Fig. 10.8. The rotational component of L_z is not large, but it does lead to an observable effect in the angular velocity of the cloud. Figure 10.9 shows that viscosity leads to a decrease in $\dot{\Theta}$. During most of the evolution this effect is dominated by the delayed expansion, but for $t \simeq t_{45^\circ}$ there is an extra reduction which is due to an increase of the effective moment of inertia $I = L/\dot{\Theta}$ caused by the rotational

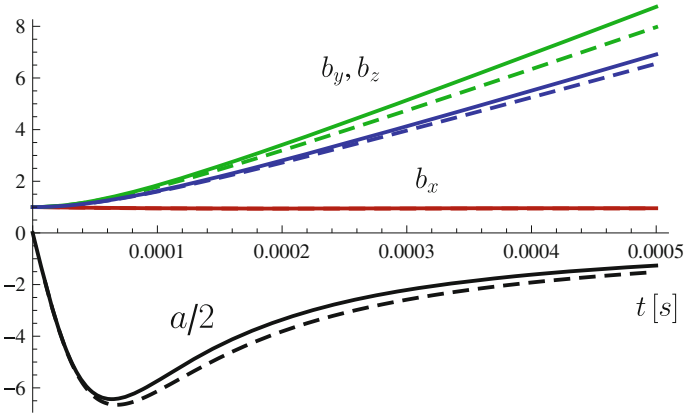

Fig. 10.6 Time evolution of the parameters a, b_x, b_y, b_z that characterize the scaling expansion out of a rotating trap. Note that in this case ω_y and ω_z are not exactly equal, and that the time scale is different from Fig. 10.5. Here, we only show the early evolution of the system. *Solid lines* show the solution of the Euler equation, and *dashed lines* show the solution of the Navier–Stokes equation for $\beta = 0.077$

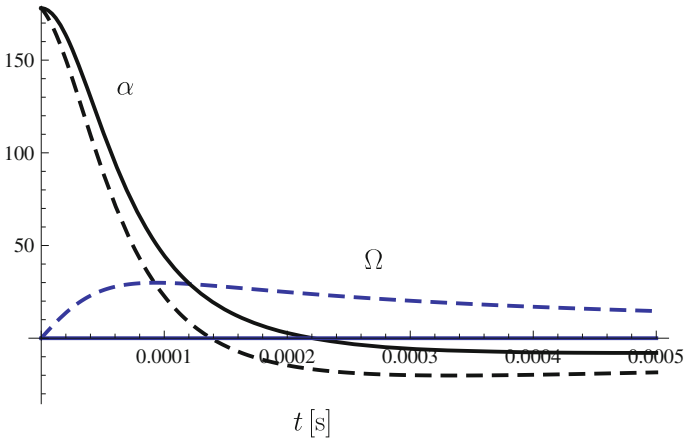

Fig. 10.7 Time evolution of the parameters α and Ω which control the irrotational and rotational components of the velocity field. Parameters were chosen as in Fig. 10.6. *Solid lines* show the solution of the Euler equation, and *dashed lines* show the solution of the Navier–Stokes equation for $\beta = 0.077$

flow. Unfortunately, the experimental data are for $\Theta(t)$ are not sufficiently accurate to demonstrate this effect.

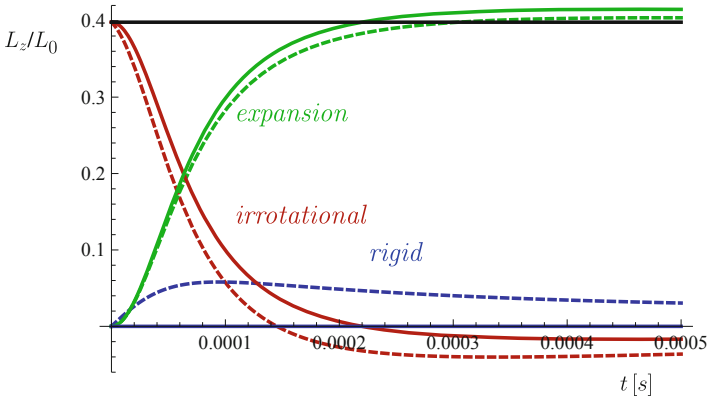

Fig. 10.8 This figure shows different contribution to the total angular momentum of the expanding cloud as a function of time. The angular momentum is given in units of the quantity L_0 defined in the text. The curves labeled irrotational, rigid, and expansion show the $\langle x^2 - y^2\rangle$, $\langle x^2 + y^2\rangle$, and $\langle xy\rangle$ contributions. The *solid* and *dashed lines* correspond to ideal and viscous hydrodynamics, respectively. The *solid black line* shows the (conserved) total angular momentum

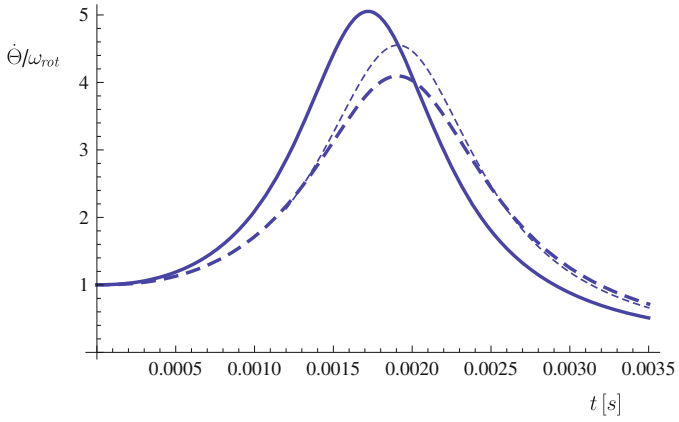

Fig. 10.9 This figure shows the angular velocity of the rotating cloud as a function of time. The *solid line* shows the solution of the Euler equation, and the *dashed line* is the solution of the Navier–Stokes equation for $\beta = 0.077$. The *thin dashed line* shows the result for the angular velocity obtained by rescaling the solution of the Euler equation by a factor $1 + (\delta t/t)_{45^\circ} \simeq 1.1$. The discrepancy between the Navier–Stokes prediction and the rescaled Euler result in the regime where $\dot{\Theta}$ is large is due to the rotational component of the flow. We note that $I = L/\dot{\Theta}$ is the moment of inertia

10.5 Collective Oscillations

In order to study collective oscillations we consider the Euler equation (10.19) in the presence of the trapping potential. The equation of motion is

$$\ddot{b}_i = \frac{\omega_i^2}{(b_x b_y b_z)^{2/3}} \frac{1}{b_i} - \omega_i^2 b_i . \tag{10.86}$$

The equilibrium solution is $b_x = b_y = b_z = 1$. We now consider small oscillations around the equilibrium, $b_i(t) = 1 + a_i e^{i\omega t}$. The linearized equation of motion gives

$$\omega^2 a_i = \omega_i^2 \left(2a_i + \gamma \sum_j a_j \right), \tag{10.87}$$

which was derived in [34, 35, 36] using slightly different methods. For the radial breathing mode $a_y = a_z = a_\perp, a_x = 0$ we get $\omega^2 = 2(1 + \gamma)\omega_\perp^2 = (10/3)\omega_\perp^2$. The energy dissipated can be computed from Eq. 10.27. We find

$$\frac{\Delta E}{E_{osc}} = -4\pi \sqrt{\frac{3}{10}} \beta \simeq -6.88 \cdot \beta, \tag{10.88}$$

where ΔE is the energy dissipated per period, E_{osc} is the energy of the collective mode, and β is the parameter defined in Eq. 10.33. We note that the amount of energy dissipated in one period of the transverse breathing mode is about three times larger than the energy dissipated by transverse expansion, see Eq. 10.32.

We can also derive a Navier–Stokes equation, either by taking moments as in Sect. 10.3.2, or by using a simple scaling form of the shear viscosity as in Sect. 10.3.3. For the transverse breathing mode we find

$$\ddot{b}_\perp = \frac{\omega_\perp^2}{b_\perp^{7/3}} - \omega_\perp^2 b_\perp - \frac{2\beta\omega_\perp \dot{b}_\perp}{b_\perp^2}. \tag{10.89}$$

If β is small then this equation is approximately solved by a damped oscillating function. We have

$$b_\perp(t) = 1 + a_\perp \cos(\omega t) \exp(-\Gamma t). \tag{10.90}$$

Comparison with Eq. 10.88 gives $\Gamma = \beta\omega_\perp$. The main feature of collective modes is that the viscous term exponentiates so that even very small values of β are experimentally accessible. In Fig. 10.10 we show a comparison between an exact solution of Eq. 10.89 for $\beta = 0.05$, $a_\perp(0) = 0.25$ and the approximate solution (10.90). We observe that the approximate solution is extremely accurate.

The experimentally measured damping rate can be used to estimate $\langle \alpha_s \rangle$. We have

$$\langle \alpha_s \rangle = (3\lambda N)^{1/3} \left(\frac{\Gamma}{\omega_\perp} \right) \left(\frac{E_0}{E_F} \right) \left(\frac{N}{S} \right). \tag{10.91}$$

In Fig. 10.11 we show an analysis of the data obtained by Kinast et al. [9] using Eq. 10.91. This plot is very similar to our earlier analysis [37] (see also [38, 39]),

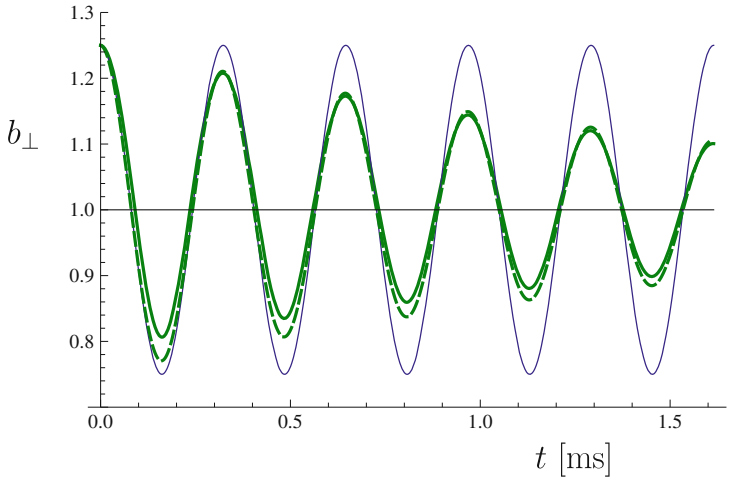

Fig. 10.10 Time evolution of the amplitude of the transverse breathing mode. The *black line* shows the solution of the Euler equation and the *solid green line* is the solution of the Navier–Stokes equation for $\beta = 0.05$. The *dashed green line* is the damped cosine function given in Eq. 10.90. The trap frequency was chosen to be $\omega_\perp = 1696$ Hz as in [10]

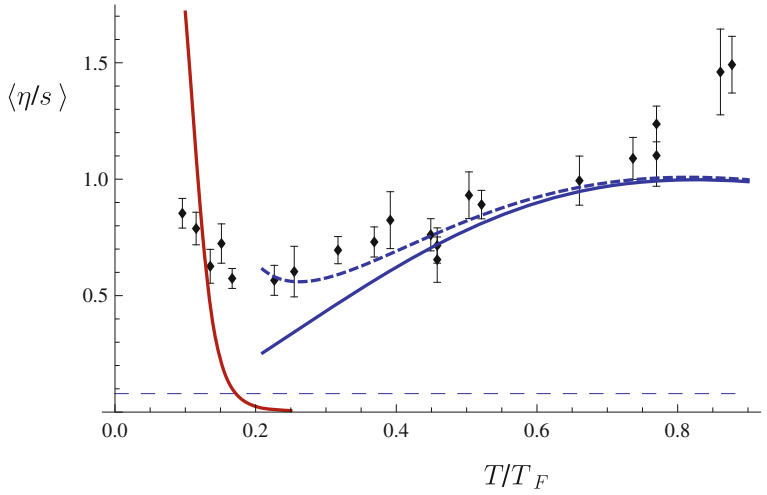

Fig. 10.11 Trap average $\langle \alpha_s \rangle = \langle \eta/s \rangle$ extracted from the damping of the radial breathing mode. The data points were obtained using Eq. 10.91 to analyze the data published by Kinast et al. [9]. The thermodynamic quantities (S/N) and E_0/E_F were taken from [22]. The *solid red* and *blue lines* show the expected low and high temperature limits. Both theory curves include relaxation time effects. The *blue dashed curve* is a phenomenological two-component model explained in the text

except that the temperature calibration and thermodynamic data have been updated using the recent analysis published in [22].

There are a number of important checks on the interpretation of the damping date in terms of viscous hydrodynamics that should be, or have already been, performed. Viscous hydrodynamics predicts that the monopole mode in a spherical trap is not damped at all. This prediction is quite striking, but it has never been tested. Viscous hydrodynamics also predicts simple relationships between the damping constant of the radial breathing mode and the radial quadrupole as well as the scissors mode [37]. These predictions agree qualitatively with the data obtained by the Innsbruck group, but there are some structures in the data that do not fit a simple hydrodynamic description. Finally, hydrodynamics predicts that the damping rate decreases as $N^{-1/3}$. This prediction does not agree with the data published in [9]. We note, however, that Kinast et al. only checked the scaling behavior at very low temperature, and that relaxation time effects may modify the particle number scaling.

We can also compare the results in Fig. 10.11 to theoretical prediction for the shear viscosity in the low and high temperature limit. In the high temperature limit the viscosity is independent of density and the main source of dissipation is the finite relaxation time, see Sect. 10.3.5. In the case of periodic motion the relaxation time equation (10.59) is easily solved. The dissipated energy is given by Eqs. 10.33, 10.88 with

$$\langle \alpha_n \rangle = \eta_0 (mT)^{3/2} \int d^3x \frac{1}{1+\omega^2 \tau_R(n(x))^2}. \tag{10.92}$$

We will use the kinetic theory result $\tau_R(n) = \eta/(nT)$ with $\eta = \eta_0 (mT)^{3/2}$. In the high temperature (low density) limit we can use the classical expression for the density profile $n(x)$. In this case the integral over x can be done analytically. We find

$$\langle \alpha_n \rangle = -\frac{45\pi}{32}\left(\frac{T}{T_F}\right)^3 Li_{3/2}\left(-\left[\frac{const}{(\lambda N)^{2/3}}\left(\frac{T}{T_F}\right)^4\right]^{-1}\right), \tag{10.93}$$

where $const = 1125 \cdot 3^{1/3}\pi^2/64 \simeq 250.1$, and $Li_\alpha(x)$ is the polylogarithm function. In the limit $T \ll T_F$ the result scales as $\langle \alpha_n \rangle \sim y^3 \log(y)^{3/2}$ with $y = T/T_F$. For $T \gg T_F$ we get $\langle \alpha_n \rangle \sim y^{-1}$. These results imply that both the temperature scaling and the particle number scaling differ from naive expectations. The shear viscosity scales as $\eta \sim T^{3/2}$, but $\langle \alpha_n \rangle \sim T^3 \log(T)^{3/2}$ at low T, and $\langle \alpha_n \rangle \sim T^{-1}$ at high T. Also, the scaling of the damping rate with N is $\Gamma \sim N^{-1/3} \log(N)^{3/2}$ at low T and $\Gamma \sim N^{1/3}$ at high T, see Fig. 10.12. This implies that there are temperature regions in which the dependence of the damping rate on N is small.

The prediction of Eq. 10.93 is shown as the solid blue line in Fig. 10.11. We observe that the relaxation time model agrees well with the data for $T \sim (0.5 - 0.8)T_F$. For temperature less than $0.5T_F$ the observed damping rate is bigger than the prediction of the relaxation model. At very low temperature the shear viscosity is expected to be dominated by the phonon contribution [23]

$$\eta = 0.018 n \left(\frac{n^{2/3}}{mT}\right)^5. \tag{10.94}$$

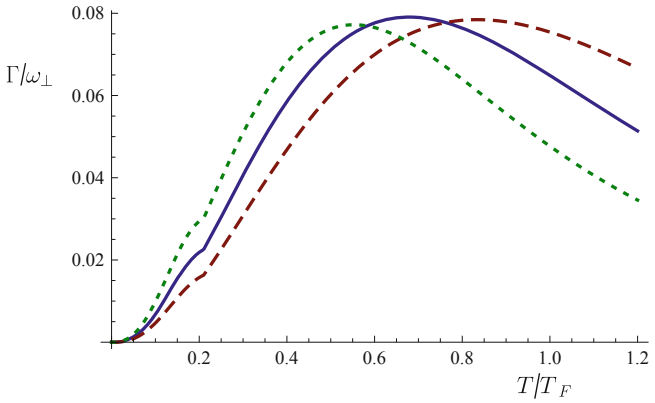

Fig. 10.12 Damping rate of the radial breathing mode in units of the transverse trapping frequency. This figure only shows the contribution from the dilute corona, computed using the relaxation time approach. The *solid line* corresponds to $N \equiv N_0 = 2 \cdot 10^5$, $\lambda = 0.045$ as in [9]. The *long dashed* and *short dashed lines* corresponds to $N = 5N_0$ and $N = 0.2N_0$, respectively

At low temperature we can compute the trap average by using the zero temperature profile. We find $\langle \alpha_n \rangle \simeq 1.5 \cdot 10^{-5}(T_F/T)^5$. This result becomes large for $T/T_F < 0.1$. In this regime relaxation time effects are important, and $\langle \alpha_n \rangle$ at finite frequency goes to zero as $T \to 0$.

Neither the low temperature nor the high temperature result provide a good description of the data in the regime $T \simeq (0.15 - 0.40)T_F$. The dashed blue line in Fig. 10.11 shows a purely phenomenological fit based on the functional form $\eta = \eta_0(mT)^{3/2} + \eta_1 n^{5/3}/(mT)$ with $\eta_0 = 15/(32\sqrt{\pi}) \simeq 0.264$ and $\eta_1 \simeq 0.06$. In this case the minimum value of η/n is 0.24 which occurs below the phase transition at $mT/n^{2/3} \simeq 0.47$.

10.6 Summary and Outlook

A special feature of the hydrodynamics of a unitary Fermi gas is the existence of simple scaling solutions of the equations of ideal fluid dynamics. These solutions are independent of the equation of state, the initial temperature and the number of particles. The only time scales in the problem are the trap frequencies, see Fig. 10.13. The existence of scaling solutions is related to the constraints imposed by scale invariance on the equation of state, and to the harmonic character of the confinement potential.

The properties mentioned above make scaling flows an ideal class of solution to study the effects of shear viscosity. In this contribution we focused on three classes of experiments, expansion from a deformed trap ("elliptic flow"), expansion from a rotating trap, and damping of collective oscillations. These experiments provide

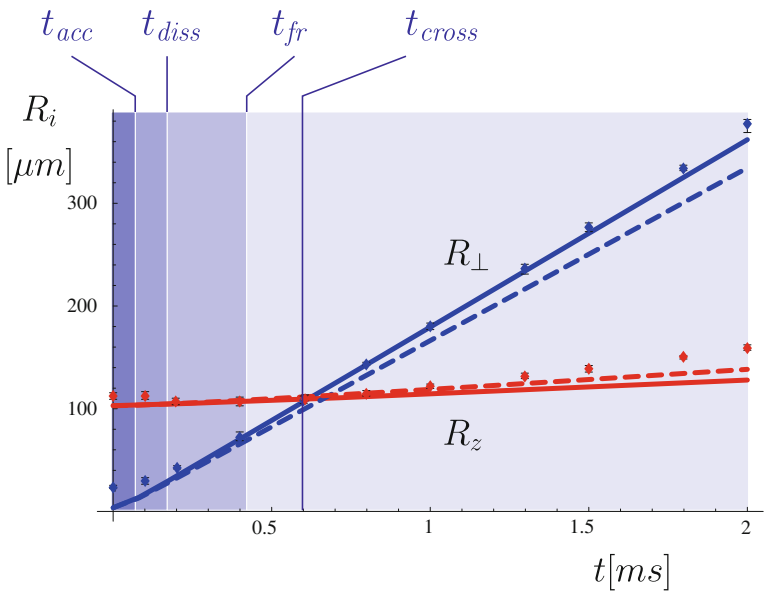

Fig. 10.13 Time scales relevant to the expansion of a unitary Fermi gas from a deformed trap. The inverse trap frequency is $\omega_\perp^{-1} = 0.024$ ms. The scale t_{acc} is the characteristic time for hydrodynamic acceleration, where we have defined $t = t_{acc}$ to be the time when 80% of the initial internal energy has been converted to kinetic energy. The characteristic time for viscous effects, t_{dis}, is determined by the condition that the dissipated energy ΔE has reached 80% of its asymptotic value. The freezeout time t_{fr} is quite uncertain. Here, we show the time at which, for $T_0/T_F = 0.21$, the freezeout surface reaches the point $x_\perp = b_\perp R_\perp$. The crossing time t_{cr} is the time at which the system becomes spherical. The time t_{3d} at which the expansion becomes three-dimensional is bigger by another factor λ^{-1}

somewhat complementary information, and they have different advantages and disadvantages:

- In the case of collective modes the effect of shear viscosity exponentiates, and as a consequence the damping of collective modes is sensitive to very small values of the shear viscosity. Collective modes also have the advantage that qualitatively the effect of dissipation is very simple: The kinetic energy of the collective mode is converted to heat, so that at the end of the evolution the system is again stationary, but the temperature is increased. In the case of flow experiments the situation is more complicated. Dissipation converts kinetic energy into heat but unless the system freezes out first, the internal energy is eventually converted back to kinetic energy. Because of the second law of thermodynamics, the final state of viscous hydrodynamics must differ from that of ideal hydrodynamics, but the differences can be subtle, manifesting themselves in violations of the simple scaling formulas for the density and the velocity field.

- The transverse expansion experiments provide detailed information about the time dependence of the density and flow profiles. This information can be used to understand the breakdown of hydrodynamics, for example by studying deviations from the simple linear velocity profile predicted by ideal fluid dynamics. Transverse flow experiments may also show a different, and possibly smaller, sensitivity to relaxation effects. Figure 10.4 shows that, for $T/T_F < 0.4$, the relaxation time estimate of the trap averaged dissipation due to the spatially constant part of the shear viscosity is similar for transverse flow and transverse collective modes. However, the local response of a rapidly expanding cloud is likely to be different from that of an oscillating system.
- The expansion of a rotating cloud is sensitive to a new viscous effect, the conversion of an irrotational flow $\vec{v} \sim \vec{\nabla}(xy)$ to a rotational flow $\vec{v} \sim \hat{z} \times \vec{x}$. Contrary to the slowdown of the transverse expansion, which could in principle be due to scale-breaking terms in the pressure or residual external potentials, this is a genuine dissipative effect, since vorticity is conserved in ideal hydrodynamics.

The main difficulty in extracting the shear viscosity from the analysis of scaling flows is associated with the role of the dilute corona of the cloud. Kinetic theory predicts that in the dilute limit the shear viscosity is independent of density and only depends on temperature. A simple analysis of the type presented in Sect. 10.3.3 then implies that the dilute corona does not generate a dissipative force. It nevertheless dissipates a large amount of energy. The analysis also suggests that freezeout only occurs very late, see Sect. 10.3.4. There are a number of aspects of this analysis that need to be improved:

- The Navier–Stokes equation is based on the assumption that the viscous correction to the stress tensor appears instantaneously. This is particularly problematic in the case of scaling flows, because the viscous contribution is spatially constant. The fact that the ideal stresses propagate outward with the expansion of the system whereas the dissipative stresses appear immediately indicates that causality is violated. This problem can be addressed by including a finite relaxation time, or by solving a more complete set of second order hydrodynamic equations.
- We have studied the effect of dissipative forces in the Navier–Stokes equations, but we have computed the non-dissipative forces (pressure gradients) based on an approximately isentropic expansion. This procedure neglects reheating, and violates energy conservation. Reheating is important in the dilute corona, and breaks the scaling nature of the expansion.

In addition to implementing these technical improvements it is important to consider other experimental setups that are directly sensitive to the spatially constant part of the shear viscosity. One option would be to measure the attenuation of sound propagating in a very long elongated trap. Another idea would be to directly measure the decay of a shear flow in a long channel.

Finally, we summarize the existing experimental constraints on the shear viscosity of the unitary Fermi gas:

- The damping of collective oscillations constrains the trap average $\langle\eta\rangle/S \equiv \langle\alpha_s\rangle$. We find that this quantity varies between $\langle\alpha_s\rangle \simeq 1$ at $T/T_F \simeq 0.8$ and $\langle\alpha_s\rangle \simeq 0.5$ at $T/T_F \simeq 0.2$. In the regime $0.4 \leq T/T_F \leq 0.8$ the temperature dependence is consistent with $\eta \sim (mT)^{3/2}$ and a relaxation time that scales as $\tau_R \sim \eta/(nT)$. At lower temperatures an additional contribution is needed. In a simple model the minimum of the shear viscosity to density ratio is $\eta/n \simeq 0.2$.
- The expansion of a rotating cloud gives $\langle\alpha_s\rangle \simeq 0.8$ at $T/T_F \simeq 0.8$, and $\langle\alpha_s\rangle \simeq (0.0-0.4)$ at $T/T_F \simeq 0.2$ [32]. The latter results are smaller than the values extracted from collective oscillations, although the errors are also somewhat larger. It will be important to determine whether this discrepancy is due to the effects of the dilute corona, and whether the smaller values of $\langle\alpha_s\rangle$ are more representative of the shear viscosity to entropy density ratio in the core.

Note added: After the initial version of this contribution was finished dissipative effects in the expansion of a dilute Fermi gas at temperatures $T \gg T_F$ were studied experimentally by Cao et al. [40]. This work nicely demonstrates the scaling $\langle\alpha_n\rangle \sim T^3$ predicted in Fig. 10.4. Numerical solutions to the equations of dissipative hydrodynamics were studied in [41]. This work shows that quantitative estimates of the shear viscosity have to take into account the effects of reheating.

Acknowledgments This work was supported in parts by the US Department of Energy grant DE-FG02-03ER41260. We are grateful to John Thomas for many useful discussions, and to Jiunn-Wei Chen for pointing out an error in an earlier version of this contribution.

References

1. Bloch, I., Dalibard J., Zwerger, W.: Rev. Mod. Phys. **80**, 885 (2008) [arXiv:0704.3011]
2. Giorgini, S., Pitaevskii, L.P., Stringari, S.: Rev. Mod. Phys. **80**, 1215 (2008) [arXiv:0706.3360]
3. Schäfer, T., Teaney, D.: Rept. Prog. Phys. **72**, 126001 (2009) [arXiv:0904.3107 [hep-ph]]
4. Danielewicz, P., Gyulassy, M.: Phys. Rev. D **31**:53 (1985)
5. Policastro, G., Son, D.T., Starinets, A.O.: Phys. Rev. Lett. **87**, 081601 (2001) [arXiv:hep-th/0104066]
6. Kovtun, P., Son, D.T., Starinets, A.O.: Phys. Rev. Lett. **94**, 111601 (2005) [arXiv:hep-th/0405231]
7. O'Hara, K.M., Hemmer, S.L., Gehm, M.E., Granade, S.R., Thomas, J.E.: Science. **298**, 2179 (2002) [cond-mat/0212463]
8. Kinast, J., Hemmer, S.L., Gehm, M.E., Turlapov, A., Thomas, J.E.: Phys. Rev. Lett. **92**, 150402 (2004) [cond-mat/0403540]
9. Kinast, J., Turlapov, A., Thomas, J.E.: Phys. Rev. A **70**, 051401(R) (2004) [cond-mat/0408634]
10. Kinast, J., Turlapov, A., Thomas, J.E.: Phys. Rev. Lett. **94**, 170404 (2005) [cond-mat/0502507]
11. Altmeyer, A., Riedl, S., Kohstall, C., Wright, M., Geursen, R., Bartenstein, M., Chin, C., Hecker Denschlag, J., Grimm, R.: Phys. Rev. Lett. **98**, 040401 (2007) [cond-mat/0609390]
12. Altmeyer, A., Riedl, S., Kohstall, C., Wright, M., Hecker Denschlag, J., Grimm, R.: Phys. Rev. Lett. **98**, 103602 (2007) [cond-mat/0611285]
13. Wright, M.J., Riedl, S., Altmeyer, A., Kohstall, C., Sanchez Guajardo, E.R., Hecker Denschlag, J., Grimm, R.: Phys. Rev. Lett. **99**, 150403 (2007) [arXiv:0707.3593[cond-mat.other]]

14. Clancy, B., Luo, L., Thomas, J.E.: Phys. Rev. Lett. **99**, 140401 (2007) [arXiv:0705.2782 [cond-mat.other]]
15. Riedl, S., Sanchez Guajardo, E.R., Kohstall, C., Altmeyer, A., Wright, M.J., Hecker Denschlag, J., Grimm, R., Bruun, G.M., Smith, H. Phys. Rev. A **78**, 053609 (2008) [arXiv:0809.1814[cond-mat.other]]
16. Carlson, J., Reddy, S.: Phys. Rev. Lett. **95**, 060401 (2005) [cond-mat/0503256]
17. Bulgac, A., Drut, JE., Magierski, P.: Phys. Rev. A **78**, 023625 (2008) [arXiv:0803.3238 [cond-mat.stat-mech]]
18. Nascimbene, S., Navon, N., Jiang, K., Chevy, F., Salomon, C. [arXiv:0911.0747[cond-mat.quant-gas]]
19. Menotti, C., Pedri, P., Stringari, S.: Phys. Rev. Lett. **89**, 250402 (2002) [cond-mat/0208150]
20. Thomas, J.E., Kinast, J., Turlapov, A.: Phys. Rev. Lett. **95**, 120402 (2005) [cond-mat/0503620]
21. Son, D.T.: Phys. Rev. Lett. **98**, 020604 (2007) [arXiv:cond-mat/0511721]
22. Luo, L., Thomas, J.E.: J. Low Temp. Phys. **154**, 1 (2009) [arXiv:0811.1159[cond-mat.other]]
23. Rupak, G., Schäfer, T.: Phys. Rev. A **76**, 053607 (2007) [arXiv:0707.1520 [cond-mat.other]]
24. Bruun, G.M., Smith, H.: Phys. Rev. A **72**, 043605 (2005) [cond-mat/0504734]
25. Bruun, G.M., Smith, H.: Phys. Rev. A **75**, 043612 (2007) [cond-mat/0612460]
26. Garcia-Colina, L.S., Velascoa, R.M., Uribea, F.J.: Phys. Rep. **465**, 149 (2008)
27. Nikuni, T., Griffin, A.: Phys. Rev. A **69**, 023604 (2004) [cond-mat/0309269]
28. Griffin, A., Nikuni, T., Zaremba, E.: Bose-condensed gases at finite temperature. Cambridge University Press, Cambridge (2009)
29. Romatschke, P.: Int. J. Mod. Phys. E **19**, 1–53 (2010) [arXiv:0902.3663 [hep-ph]]
30. Bruun, G.M., Smith, H.: Phys. Rev. A **76**, 045602 (2007) [arXiv:0709.1617]
31. Edwards, M., Clark, C.W., Pedri, P., Pitaevskii, L., Stringari, S.: Phys. Rev. Lett. **88**, 070405 (2002)
32. Thomas, J.E.: Nucl. Phys. A **830**, 665C–672C (2009) [arXiv:0907.0140v2 [cond-mat.quant-gas]]
33. Clancy, B.: Ph.D. thesis, Duke University (2008)
34. Heiselberg, H.: Phys. Rev. Lett. **93**, 040402 (2004) [cond-mat/0403041]
35. Stringari, S.: Europhys. Lett. **65**, 749 (2004) [cond-mat/0312614]
36. Bulgac, A., Bertsch, G.F.: Phys. Rev. Lett. **94**, 070401 (2005) [cond-mat/0404687]
37. Schäfer, T.: Phys. Rev. A **76**, 063618 (2007) [arXiv:cond-mat/0701251]
38. Gelman, B.A., Shuryak, E.V., Zahed, I.: Phys. Rev. A **72**, 043601 (2005) [nucl-th/0410067]
39. Turlapov, A., Kinast, J., Clancy, B., Luo, L., Joseph, J., Thomas, J.E.: J. Low Temp. Phys. **150**, 567 (2008) [arXiv:0707.2574]
40. Cao, C., Elliott, E., Joseph, J., Wu, H., Petricka, J., Schäfer, T., Thomas, J.E.: Science **331**, 5 (2011) [arXiv:1007.2625 [cond-mat.quant-gas]]
41. Schäfer, T.: Phys. Rev. A **82**, 063629 (2010) [arXiv:1008.3876 [cond-mat.quant-gas]]